# Laboratory Simulations of Directionally Spread Shoaling Waves

By Steve Elgar,[1] R. T. Guza,[2] M. H. Freilich,[3] and M. J. Briggs[4]

**Abstract:** Field observations of a shoaling, nonbreaking, directionally spread wave field are simulated in a laboratory basin to determine whether laboratory artifacts cause significant distortions of the shoaling process. The laboratory wave field is measured with scaled arrays of surface-elevation sensors similar to the arrays used for the field observations. However, differences in the laboratory and field beach slopes (0.033 and 0.025, respectively) do not allow precise replication of the field conditions in the laboratory. Therefore, a nonlinear wave propagation model with no adjustable parameters (previously successfully compared to a wide range of field data) is used to show that differences between the laboratory and field data sets are caused primarily by the different beach slopes. The observations demonstrate, in agreement with the model, that it is possible to compensate partially for differences in beach slope by altering the initial conditions. With such compensation, the evolution of surface-elevation power spectra, bispectra, and skewness and asymmetry are remarkably similar in the laboratory and field. Frequency-directional spectra measured just outside the surf zone also show similar nonlinear effects in both field and laboratory data. Based on this case study, the laboratory directional wave basin appears to be useful for investigating the linear and nonlinear evolution of random, two-dimensional waves on beaches.

## Introduction

Ocean surface gravity waves in the wind-wave and swell frequency bands evolve substantially as they propagate shoreward on a beach. Prior to breaking, these waves are weakly dispersive and weakly nonlinear and thus, near-resonant nonlinear triad interactions result in slow cross-spectral energy transfers (e.g., the growth of harmonics) and phase coupling between different frequencies (e.g., nonsinusoidal wave shapes). Although certain statistics (e.g., significant height, peak period) of nonbreaking shoaling waves may be predicted accurately using linear wave theory, many important statistics result from nonlinearities in the wave field. In particular, third moments of sea-surface elevation and horizontal velocity, related to net sediment transport (Bjiker et al. 1976; Bowen 1980; Bailard and Inman 1981), are zero for a linear random wave field, and thus cannot be predicted with linear theory. In the general case of directionally spread random waves propagating in variable depth, both linear and nonlinear processes lead to spatial changes in the frequency-directional spectrum, $E(f,\theta)$.

Primarily owing to logistical difficulties, there have been very few field experiments designed to acquire high-resolution measurements of the spatial evolution of $E(f,\theta)$ during shoaling. The required extensive arrays of sensors

[1]Assoc. Prof. Electrical and Computer Engrg., Washington State Univ., Pullman, WA 99164-2752.

[2]Prof., Ctr. for Coastal Studies, Scripps Inst. of Oceanography A-009, La Jolla, CA 92093.

[3]Member of Tech. Staff, Jet Propulsion Lab. 300–323, Pasadena, CA 91109.

[4]Res. Hydr. Engr., Coastal Engrg. Res. Ctr., Waterways Experiment Station, Vicksburg, MS 39180.

Note. Discussion open until June 1, 1992. To extend the closing date one month, a written request must be filed with the ASCE Manager of Journals. The manuscript for this paper was submitted for review and possible publication on September 25, 1990. This paper is part of the ***Journal of Waterway, Port, Coastal, and Ocean Engineering***, Vol. 118, No. 1, January/February, 1992. ©ASCE, ISSN 0733-950X/92/0001-0087/$1.00 + $.15 per page. Paper No. 556.

are expensive and difficult to install and maintain. The (possibly changing) bathymetry must be both well surveyed and have negligible longshore variability over the array span to interpret the array data in a relatively straightforward way. Temporal nonstationarity in the wave field owing to tides or varying wave conditions may preclude obtaining data records with sufficient statistical stability.

On the other hand, modern experimental facilities have potential for the efficient study of the evolution of realistic (i.e., broad banded in frequency and direction) wave fields for a range of wave conditions and bathymetries. Temporal stationarity can be assured, sensors can easily be moved within the basin, and incident wave conditions and the bathymetry can be controlled. However, before using the laboratory for this purpose it must first be demonstrated that laboratory artifacts do not significantly distort the shoaling process. This is the purpose of the present work.

Previous studies with normally incident waves have shown that scale effects in typical laboratory wave flumes have negligible impact on the transformation of wave heights and setup of random waves, and on the temporal mean and instantaneous extreme cross-shore currents associated with periodic breaking waves (Stive 1985). Additional laboratory data have been compared to predictions based on Boussinesq wave propagation models (Abbott et al. 1978; Madsen and Warren 1984; Liu et al. 1985; Rygg 1988). Despite the success of these and other laboratory studies, there are effects that may distort the evolution of directionally spread waves in the laboratory, particularly when the wave field is nonlinear. Examples of such artifacts include low-frequency basin seiches (Bowers 1977), which may be particularly troublesome in shallow water, circulation patterns driven by dissipation and reflection at the sidewalls and beach, the high rate of viscous damping of high-frequency laboratory waves, and the finite longshore extent of the wave generator. In the present study, field observations of nonbreaking waves exhibiting significant nonlinear shoaling evolution (Freilich et al. 1990) are compared to scaled simulations of the same wave field in the laboratory. Distortions in the laboratory basin for these conditions are shown to be small. Thus, this facility may be used with greater confidence to study the evolution of wave fields for a range of $E(f,\theta)$ not observed previously in detailed field studies.

The field and laboratory experiments are described first. Next, one-dimensional (nondirectional) second and third moments from the field and laboratory are compared both to each other, and to the predictions of a numerical wave propagation model with no free parameters. Agreement is good. Finally, field and laboratory measurements of $E(f,\theta)$ are qualitatively compared, and the same important features are shown to be present in both cases.

## Experimental Design

### Field Data

A shoaling wave field observed at Torrey Pines Beach, California was simulated in the laboratory. Parameters of the field and laboratory data sets are summarized in Table 1 and discussed in detail herein.

Field estimates of $E(f,\theta)$ were obtained from longshore arrays of six bottom-mounted pressure sensors (~10-m water depth, 395-m array length) and six surface-piercing wavestaffs (~4-m depth, 190-m array length), as shown in Fig. 1. The bottom contours were nearly plane and parallel, with

**TABLE 1. Parameters for Field and Laboratory Experiments**

| Item (1) | Parameter (2) | Field (3) | Laboratory (4) |
|---|---|---|---|
| Deep array | $H$ (cm) | 72.0 | 0.8,2.2,3.4,6.8 |
| | $f_p$ (Hz) | 0.062 | 0.37 |
| | $h$ (m) | 10.3 | 0.31 |
| | $k_p h$ | 0.41 | 0.43 |
| | $k_p L$ | 0,1.2,3.2,3.9,9.2,15.7 | 0,4.2,5.8,8.3,9.2,15.8 |
| Shallow array | $h$ (m) | 4.1 | 0.12 |
| | $k_p h$ | 0.25 | 0.26 |
| | $k_p L$ | 0,4.8,5.5,7.3,8.4,11.8 | 0,4.6,6.3,9.3,10.0,17.1 |
| Cross shore | $\Delta x$ (m) | 246 | 5.4 |
| | $\int (k_p/2\pi)dx$ | 1.9 | 1.4 |
| | Slope | 0.025 | 0.033 |
| Sampling | Degrees of freedom | 320 | 250 |
| | Record length (hr) | 5.7 | 0.71 |
| | $\Delta f$ (Hz) | 0.0078 | 0.049 |
| | $f_p/\Delta f$ | 8 | 8 |

Note: Significant wave height at deep array (located in depth $h$) is $H$; the wavenumber of the power spectral primary peak frequency ($f_p$) is $k_p$; $L$ is sensor alongshore position, $\Delta x$ is cross-shore separation of arrays, $\int (k_p/2\pi)dx$ is scaled $\Delta x$; and $\Delta f$ is final frequency resolution.

a mean beach slope of 0.025 over the 246-m cross-shore distance between the arrays. The deep array had dimensionless longshore separations (i.e., lags) of approximately 2-3-1-8-10 between adjacent sensors, with unit lag of 16.5 m. The shallow array had longshore lags of approximately 8-1-3-2-5 with unit lag of 10 m, and had resolution comparable to the deep array, after accounting for the effects of linear refraction.

Nondirectional properties (e.g., power spectra and bispectra) were estimated with point measurements along a transect separating the arrays. The instruments were sampled at 2 Hz for about 5.7 hours. The frequency spectrum, averaged over all sensors in the deep array, is shown in Fig. 2. Based on the total measured variance at the deep array, the significant wave height was 72 cm. Power and cross spectra were smoothed to a final frequency resolution of 0.0078 Hz with 320 degrees of freedom. This is a unique data set owing to the simple bathymetry, high-resolution arrays, and good statistical stability. The overall experiment design is described in Freilich and Guza (1984), and details of the data processing methods are given in Freilich et al. (1990).

**Laboratory Basin Description**

The laboratory basin is located at the U.S. Army Engineer Waterways Experiment Station's Coastal Engineering Research Center and is described in detail by Briggs et al. (1987), Briggs and Hampton (1987), Vincent and Briggs (1989), and references therein. As configured for this study, the basin had dimensions of approximately 35 m alongshore by 29 m cross shore, with a 0.033 slope beach extending about 10-m seaward from the still-water shoreline to the constant depth portion of the basin (Fig. 1). The wave

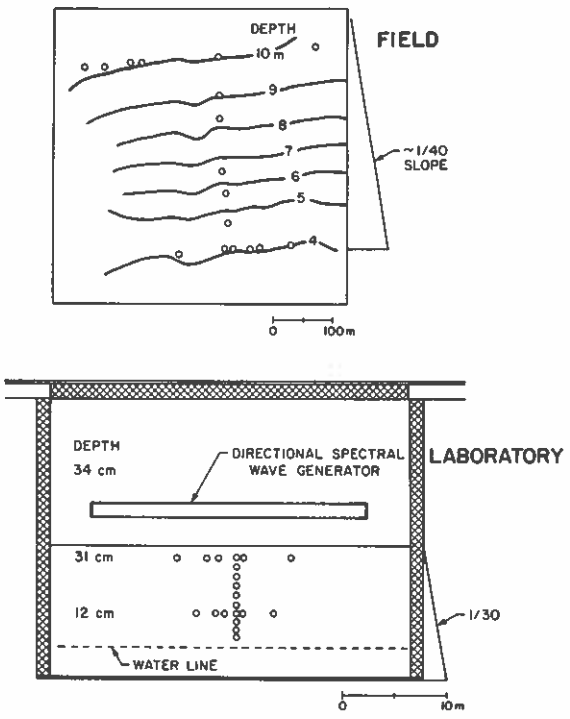


**FIG. 1. Plan Views of Experiments. Circles Indicate Wave Height Sensors, Lines in Upper Panel are Bottom Contours, and Cross-Hatching Indicates Wave Absorbers**

generator was 3-m seaward of the toe of the sloping concrete beach, in a constant depth of 34 cm. The directional spectral wave generator was 27.43 m long and consisted of 60 paddles, each 46 cm wide and 76 cm high. Electric motors individually drove each of the 61 paddle joints in translational motion. Flexible plastic plate seals slid in guides between each paddle to provide continuity, and the gap between the basin floor and the paddles was less than 1 cm, thus reducing secondary flows. Reflections at the basin sidewalls were reduced with wave absorbers. On one side of the basin, the absorbing material was placed in a trench backed by a concrete wall, while on the opposite side of the basin, the absorbing material formed a permeable boundary with an adjacent basin.

Capacitance-type wave elevation sensors (Briggs and Hampton 1987) were sampled at 10 Hz for 0.71 hours for each data set. The sensors were calibrated at least twice per day by physically moving their holding rods through a series of 11 vertical steps, with calibration coefficients obtained by a least-squares fit. These calibrations confirmed that the gauges were stable and linear. Statistics presented below are averages over 25 short records of 102.4-s duration and five neighboring frequency bands, with a frequency resolution of 0.049 Hz and 250 degrees of freedom.

**Laboratory Initial Power Spectra**

The frequency dependence of the laboratory power spectrum was a linearly scaled version of the field power spectrum. The laboratory and field

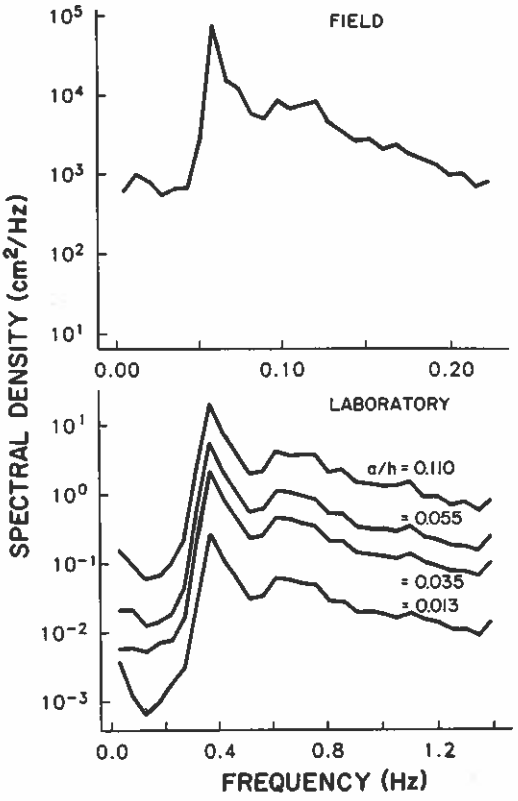


**FIG. 2. Autospectra of Water-Surface Elevation Observed at Deep Arrays**

power spectral primary peaks were at $f_p = 0.37$ Hz and $f_p = 0.067$ Hz, respectively (Fig. 2). Thus, with laboratory and field frequency resolution of 0.049 Hz and 0.0078 Hz, respectively, both spectral peaks are in frequency band No. 8. All subsequent references to frequency are given in units of band number. At each frequency band, the target laboratory distribution of energy as a function of direction was equal to the field estimate. Gain controls in the paddle electronics enabled the amplitude of the paddle drive signals to be linearly adjusted, allowing the generation of wave fields with nearly identical frequency-directional spectral shapes, but different total energy levels. Gains ranging over a factor of eight were used. Power spectra are shown in Fig. 2 for gains corresponding to deep-water $a/h$ values of 0.013, 0.035, 0.055, and 0.110, where $a$ is the significant amplitude and $h$ is the depth ($h = 31$ cm) at the deep array. In the field, the analogous $a/h = 0.036$. The smallest gain produced a wave field with nearly linear evolution between the deep and shallow arrays (shown below), while the largest gain produced waves that frequently broke seaward of the shallow array (breaking was not observed between the arrays in the field experiment).

**Laboratory Arrays**

Ideally, the laboratory waves and sensor arrays should be scaled replicas of the field experiment. Although some similitude was achieved, exact rep-

lication was not possible owing to the different beach slopes (0.033 laboratory, 0.025 field). However, as discussed in the next section, a nonlinear wave propagation model based on the Boussinesq equations and having no free parameters allows quantitative comparison of laboratory and field data.

The laboratory deep array was located 4 m shoreward of the wave generator, 1 m up the slope, in a depth of 31 cm (Fig. 1). This location was many water depths and wave-paddle widths shoreward of the wave generator so near-field effects associated with the wave generator were small, as were shoaling effects between the wave generator and the deep array. At the deep array, the laboratory and field had nearly equal $k_p h$ values (0.43 and 0.41, respectively), where $k_p$ is the wave number of the power spectral primary peak frequency given by linear theory. The laboratory deep array had an 8-1-3-2-5 lag configuration, similar to the field shallow array. The unit lag (0.60 m) was selected so that the deep laboratory array had the same normalized length (scaled by the wavelength of the spectral peak, $\lambda_p$) as the deep field array (Fig. 3). Model testing showed that the 8-1-3-2-5 lag configuration of the deep laboratory array gave slightly better directional estimates than the 2-3-1-8-10 field deep array for the particular directional distributions studied here.

The shallow laboratory array was located in 12 cm depth where $k_p h = 0.26$, compared to $k_p h = 0.25$ for the shallow field array. The shallow laboratory array had the same 8-1-3-2-5 lag configuration as the shallow field array. However, the unit lag for the shallow laboratory array was 0.41 m, yielding a longer normalized array length than the field array. Simulations show that the field and laboratory arrays have similar resolution despite differences in details of the array configurations.

On mildly sloping beaches with plane parallel contours, linear shoaling and refraction depend only on $kh$, and not on the beach slope. Thus, if linear effects dominated the evolution between the arrays, laboratory and field frequencies with equal band number (and hence equal $kh$ at the cor-

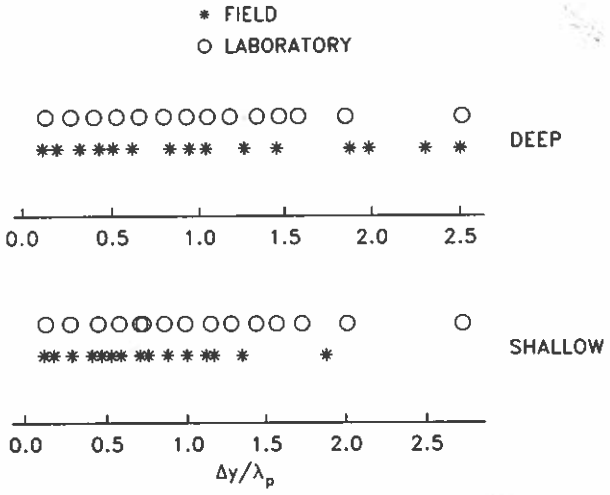


**FIG. 3. Longshore Separation between Pairs of Longshore Array Sensors ($\Delta y$), Normalized by Wavelength ($\lambda_p$) of Autospectral Primary Peak Frequency**

responding arrays) would show equal amplification and refraction. With sensor arrays of comparable resolution, and $E(f,\theta)$ at the deep arrays related by the linear scaling described previously, $E(f,\theta)$ at the shallow arrays would be related by a single constant factor.

Nonlinear effects, however, depend on propagation distance and wave amplitude as well as on $kh$. The cross-shore separation between the deep and shallow arrays was 5.4 m in the laboratory and 246 m in the field, corresponding to normalized cross-shore separations [$\int_{x_d}^{x_s} (k_p/2\pi)dx$, where $x_d$ and $x_s$ are the cross-shore coordinates of the deep and shallow arrays] of approximately 1.4 and 1.9 in the laboratory and field, respectively. The smaller, normalized separation between the laboratory arrays resulted from the larger laboratory beach slope and the positioning of the laboratory arrays such that $k_ph$ was equal to the field value at each array. For equal $a/h$ (0.036) and $k_ph$ at the deep arrays, the shorter normalized separation in the laboratory indeed resulted in somewhat less nonlinear evolution than was observed in the field.

However, increasing the initial amplitude of the laboratory waves increases the strength of nonlinear interactions, and thus may compensate for the shorter relative distance between deep and shallow arrays. The theory based on the Boussinesq equations [e.g., Mei and Ünlüata (1972)] illustrates the importance of propagation distance and provides a qualitative estimate of the required change in initial amplitude. In the special case of a wave field consisting primarily of a single wave train (amplitude = $a_p$, frequency = $f_p$), the initial evolution of a small harmonic amplitude ($a_2$, frequency = $2f_p$) in constant depth is

$$a_2(x) = a_p\left(\frac{a_p}{h}\right)f(k_ph)(k_px) + a_2(0) \quad \ldots\ldots\ldots\ldots\ldots\ldots\ldots\ldots (1)$$

where $f(k_ph)$ = a function of $k_ph$; $a_2(0)$ = the initial amplitude of th harmonic; and $k_px$ = the nondimensional propagation distance from $x$ = 0. Eq. (1) is the small amplitude ($a_2 << a_p$), short evolution distance [$k_px << (k_ph)^{-2}$] limit of the solution of Mei and Ünlüata (1972). In this special case, $a_2$ grows linearly with $x$.

The scaling used was such that $k_ph$ was the same for field and laboratory at the deep and shallow arrays. Thus, an approximately constant ratio of $a_2/a_p$ (i.e., the same spectral shape) for cases of different evolution distance requires $(a_p/h)k_px \sim$ constant. The ratio of the propagation distances was $\tan(\beta_{lab})/\tan(\beta_{field}) = 0.033/0.025 = 1.32$ where $\beta$ is the beach slope. Thus, according to (1), $(a/h)_{lab} = 1.32(a/h)_{field} = 0.048$ for comparable spectral evolution at the shallow arrays.

This scaling is only approximate because it is based on constant depth and simplified physics (small evolution distances, a single plane wave with only one [small] harmonic, and a constant primary amplitude). Nonlinear model simulations (discussed herein) of a spectrum of waves propagating over the 1/30 laboratory beach slope for $a/h = 0.048$ and $a/h = 0.055$ had evolution similar to each other and to the field data. However, the nonlinear model simulations suggested that $a/h = 0.055$ may result in closer agreement between the field and laboratory data. Consequently, $a/h = 0.055$ was chosen for the amplitude of the laboratory waves.

Exact scaling of all three parameters ($a/h$, $kh$, $\int k_p dx$) cannot be simply achieved with different laboratory and field beach slopes. The numerical model described herein is used to show that the observed differences in evolution with similar $a/h$ (~0.036), and the approximate compensation for

differing beach slopes achieved by increasing the amplitude of the laboratory waves to $a/h = 0.055$, is consistent with theory and is not a result of laboratory artifacts.

## Laboratory-Field-Model Comparisons

In this section the shoaling evolution observed in the laboratory and field are compared to each other and to a numerical model for the propagation in variable depth of a wave field with arbitrary power spectrum based on the nonlinear Boussinesq equations [Freilich and Guza (1984) and references therein]. The Boussinesq model includes linear effects, which depend only on $kh$; and nonlinear terms, which depend on $kh$, wave amplitudes, phases, and evolution distance. First, power spectra, bispectra, and third moments are compared. The wave propagation model has been shown previously to predict these statistics accurately in field data (Freilich and Guza 1984; Elgar and Guza 1985*a*, 1986; Elgar et al. 1990). Model-data comparisons are restricted to one-dimensional (i.e., nondirectional) quantities because the model assumes the waves are normally incident. Although details of the beach slope do not effect qualitatively the nonlinear evolution of the wave field (Freilich and Guza 1984), the different beach slopes in the field and laboratory experiments resulted in different normalized evolution distances between the respective deep and shallow arrays for the $kh$ scaling used. This difference must be accounted for in detailed quantitative comparisons between field and laboratory data. The comparisons show that the differences between the observed shoaling evolution in the laboratory and field are not caused by laboratory artifacts, but by differences in the evolution distance owing to differences in the beach slope and the placement of the arrays. The agreement between laboratory data and model predictions is very similar to the agreement between field data and model predictions. The one-dimensional model-data comparisons are followed by a qualitative comparison of $E(f,\theta)$ at the field and laboratory shallow arrays.

Power spectral shapes at the deep array in the laboratory are similar to those observed in the field, as shown in Fig. 4. The power spectra of water-surface elevation in Fig. 4 are averages over the six sensors in each deep array, and are scaled by the total variance (the unnormalized spectra are shown in Fig. 2). For the laboratory paddle control signal, spectral levels below frequency band No. 7 were set nearly to zero. These low frequencies are not considered here because their energy levels can be sensitive both to nonlinearities in the wave generation processes and to the geometry and reflectivity of the basin boundaries (e.g., Bowers 1977). A result of the present study is that the shoaling of higher frequency waves seawards of the surf zone is not significantly altered by laboratory artifacts at low (infragravity) frequencies.

For frequencies above band No. 15, the spectral levels at the laboratory deep array are somewhat greater than the corresponding field values (Fig. 4). However, small variations at high frequencies at the deep array (where spectral densities are relatively low) do not have significant effects for the shoaling evolution discussed here, and in any event are accounted for in the initial conditions used in the numerical model. As expected for this well-calibrated facility, in the energetic part of the spectrum there are only small differences between the normalized power spectra measured at the laboratory deep array (for all gains) and the desired spectral shape.

The shoaling evolution of the power spectrum in the laboratory and field

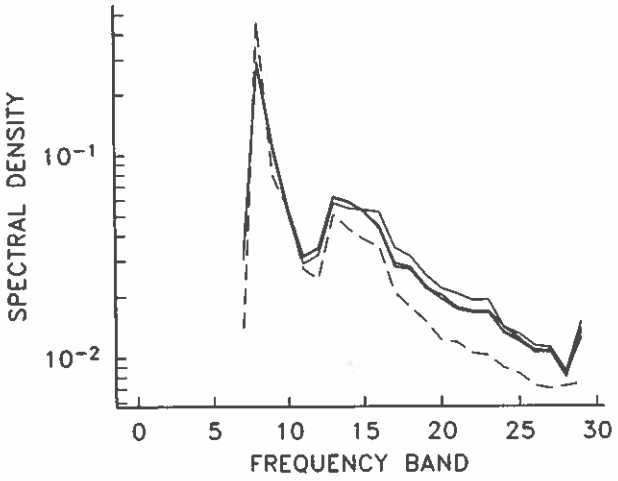


**FIG. 4. Observed Normalized Power Spectra at Deep Arrays. Solid Lines Represent Different $a/h$ Ratios in Laboratory and Dashed Line is Field Data**

is well predicted by the model (Fig. 5). Similar to Fig. 4, each shallow array spectrum in Fig. 5 has been scaled by the total power measured at the corresponding deep array. There was similar agreement between predictions and data for all the values of $a/h$ investigated (the highest and lowest values of $a/h$ are shown in Fig. 5). The agreement between observed and predicted changes in spectral shape between the deep and shallow arrays is more clearly illustrated by considering the amplification (i.e., ratio of spectral levels) between the arrays, shown in Fig. 6 for several laboratory initial wave heights. The observed amplification of the spectral levels below frequency band No. 20 for the smallest laboratory waves [$a/h = 0.013$, Fig. 6($a$)] is consistent with both the nonlinear Boussinesq model and a linear, finite-depth model (LFDT in Fig. 6). For frequencies above band No. 20, the data [and LFDT, Fig. 6($a$)] diverge from the nonlinear model because the long wave assumption underlying the Boussinesq model is increasingly violated. Nonlinear effects are negligible in this case of small amplitude waves, and LFDT performs well. Similar results of comparisons between LFDT, the nonlinear model, and field data with extremely weak nonlinearity were reported by Freilich and Guza (1984) and Elgar and Guza (1985$a$).

As $a/h$ values are increased, nonlinear effects become important and the considerable deviations from LFDT in the laboratory data are well predicted by the nonlinear model at all frequencies. For example, Fig. 6 shows that the observed growth of harmonics (bands No. 16 and 23–24) of the spectral peak (band No. 8) is strongest for the largest amplitude nonbreaking laboratory waves ($a/h = 0.055$), in agreement with the model. Note that reduced amplification relative to LFDT is observed at frequency bands No. 6–15, in accordance with model predictions. Wave breaking probably is responsible for the consistent overprediction of amplifications with the largest $a/h$ [$a/h = 0.110$, Fig. 6($d$)].

Fig. 6($b$) corresponds to laboratory $a/h = 0.035$, nearly identical to the field value of 0.036. In both cases, the amplification predicted by the Boussinesq model is very similar to that measured. Thus, in each case, the model

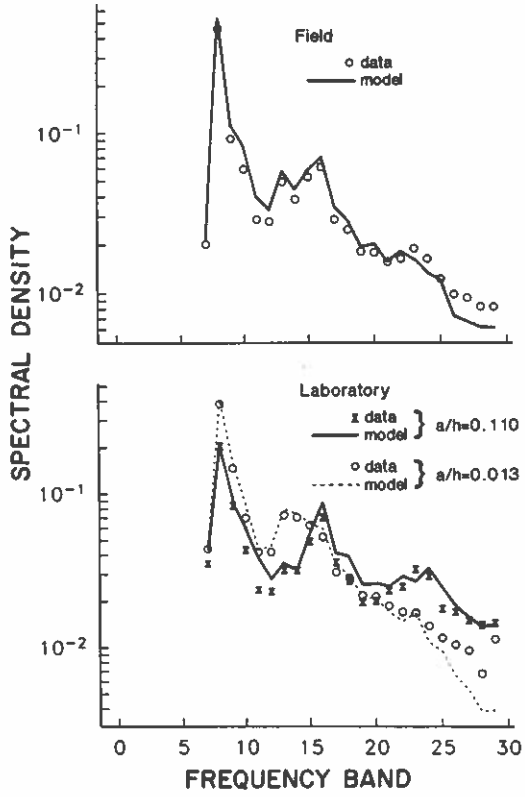


**FIG. 5. Predicted and Observed Normalized Power Spectra at Shallow Arrays**

initialized with appropriate deep-water measurements accurately predicted the corresponding shallow water observations. However, although the initial $a/h$ values are nearly the same in the laboratory and the field, the observed (and predicted) amplifications in the laboratory differ significantly from those observed (and predicted) in the field. As discussed previously, the normalized distance between the laboratory arrays is smaller than in the field, and thus the nonlinear evolution predicted (observed) for the laboratory should be less than that predicted (observed) in the field. The results shown in Fig. 6($b$) thus arise primarily from differences between the laboratory and field experimental parameters, rather than from laboratory artifacts.

Fig. 6($c$) shows the predicted and observed field amplifications for laboratory data having $a/h = 0.055$. The laboratory observations again agree well with model predictions. In this case, however, the laboratory amplifications also closely resemble the observed field amplifications. The larger amplitudes of the laboratory waves approximately compensate for their shorter normalized evolution distance.

The deep-water field observations were generally consistent with random phases, as indicated by bicoherence values not significantly different from zero (not shown). The laboratory waves were generated by coupling random

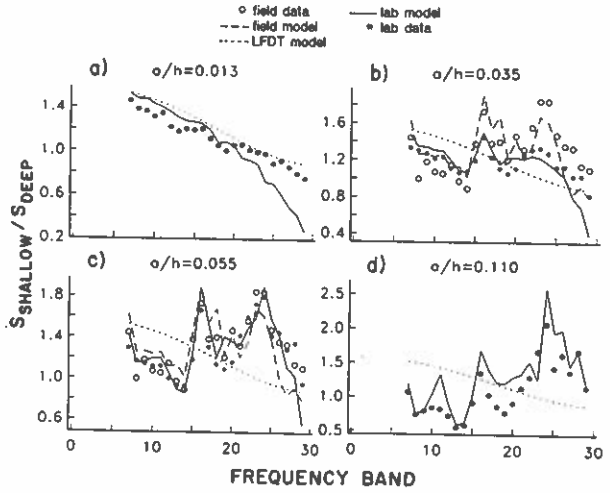


**FIG. 6. Ratio of Shallow-Water to Deep-Water Spectral Levels for Various Initial Values of $a/h$ in Laboratory (Solid Line, All Panels) and Field (Dashed Line, $a/h$ = 0.036, Panels b, c)**

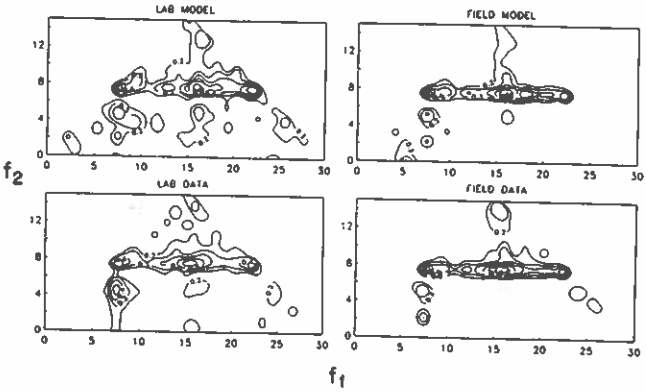


**FIG. 7. Contours of Bicoherence at Center of Shallow Arrays. Minimum Contour Plotted is $b$ = 0.2 (95% Significance Level), with Contours Every 0.1**

phases with the target frequency-directional spectrum, and bicoherences at the laboratory deep array were also essentially zero, except for the largest value of $a/h$. Although both the laboratory and field data show an absence of phase coupling between different frequencies at the deep arrays, nonlinear interactions during shoaling lead to nonrandom phase relationships between triads of waves. The strength of this phase coupling is indicated by the bicoherence [Elgar and Guza (1985*b*) and references therein], which evolves similarly in the laboratory and the field (Fig. 7 shows the case of laboratory $a/h$ = 0.055). At both the laboratory and field shallow arrays, as predicted by the model, the bicoherence spectra indicate particularly

strong nonlinear coupling between waves at the primary power spectral peak (band No. 8) and its harmonics, as well as significant coupling of the primary peak to waves at all other frequencies. This comparison further illustrates that the entire range of energetic frequencies in the laboratory (bands No. 6–30, corresponding to 0.29–1.5 Hz) undergoes shoaling evolution similar to that observed in the field.

The phase coupling indicates nonsinusoidal wave profiles. As the waves shoal, they evolve from shapes symmetric about horizontal and vertical planes at the deep arrays, to skewed (sharp peaks and flat troughs) and vertically asymmetric (steep front faces and gently sloping rear faces) profiles just before breaking. This evolution in wave shape is statistically quantified by third moments of water-surface elevation, skewness, and asymmetry (Elgar and Guza 1985*b*). As shown in Fig. 8, the evolution of water-surface elevation skewness and asymmetry observed in the laboratory for the range of $a/h$ values considered is consistent with model predictions (except for the largest waves, $a/h = 0.110$, which were breaking at the shallowest sensors and for which the model underpredicted asymmetry). The laboratory ($a/h = 0.055$) and field data ($a/h = 0.036$) agree comparably well with the model, and are notably similar to each other [Fig. 8(*c*)]. Linear theory predicts zero values of skewness and asymmetry owing to the underlying assumption of random phases.

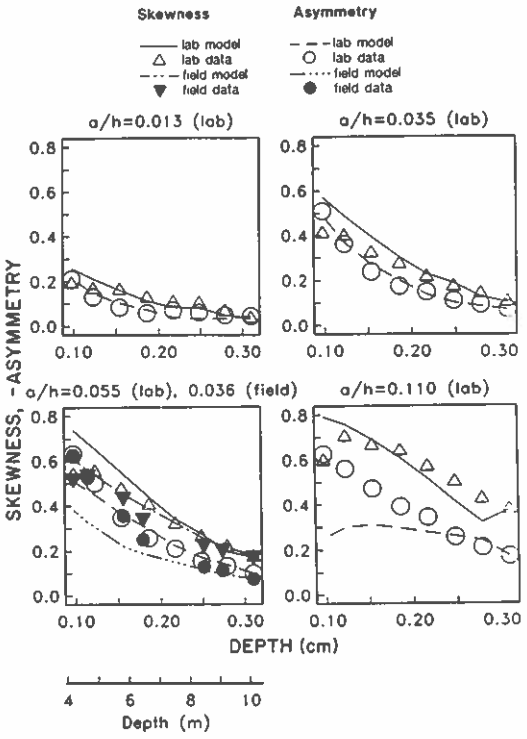


**FIG. 8. Normalized Third Moments versus Depth. Data have Been Band-Pass Filtered between Bands No. 6 and 29**

The comparisons along the cross-shore transects (Figs. 5–8) indicate that although the laboratory and field beach slopes differ, the shoaling evolution of one-dimensional quantities [that can be calculated without knowledge of $E(f,\theta)$] are similar in the laboratory and field, and differences between them are well predicted by the numerical model. Comparisons between laboratory and field observations of the shoaling evolution of $E(f,\theta)$ will now be made for the laboratory case ($a/h$ = 0.055) that most closely resembles the field data [Fig. 6($c$) and 8($c$)].

Briggs et al. (1987) have shown that the wave generator is capable of reproducing wave fields with specified directional spectra ranging from very narrow in both frequency and direction, to bimodal frequency spectra where waves at each power spectral peak were directionally spread with different central angles. Fig. 9, which shows laboratory and field directional spectra measured at the deep arrays, further illustrates the fidelity of the wave generator. For Fig. 9, the two-dimensional spectral densities are first normalized such that the one-dimensional power spectral density in each band is the same for field and laboratory. At each frequency the variance is then distributed linearly with direction, while the area under the curve at each frequency is proportional to the logarithm of the normalized autospectral density at that frequency. Details of six frequency bands are shown in Fig. 10, where the values are scaled by their respective deep water values, similar to the scaling used in Fig. 5. The directional spectra measured at the laboratory deep array are very similar to those observed in the field. At the power spectral primary peak frequency (band No. 8, Fig. 10) the deep-

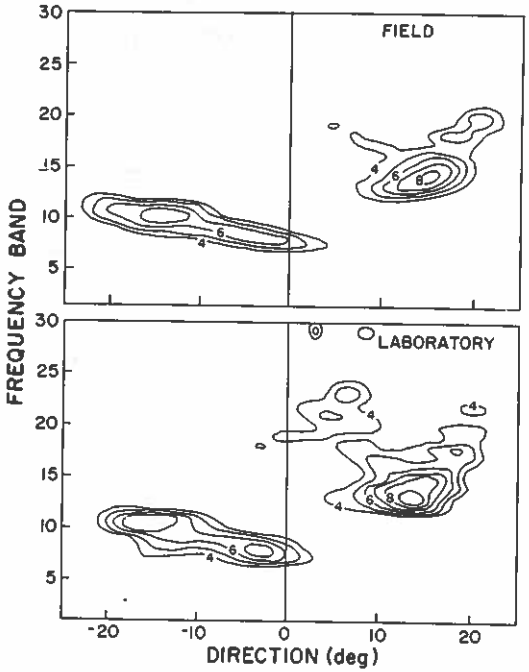


**FIG. 9. Measured Deep-Water Frequency-Directional Spectra (Laboratory Deep $a/h$ = 0.055)**

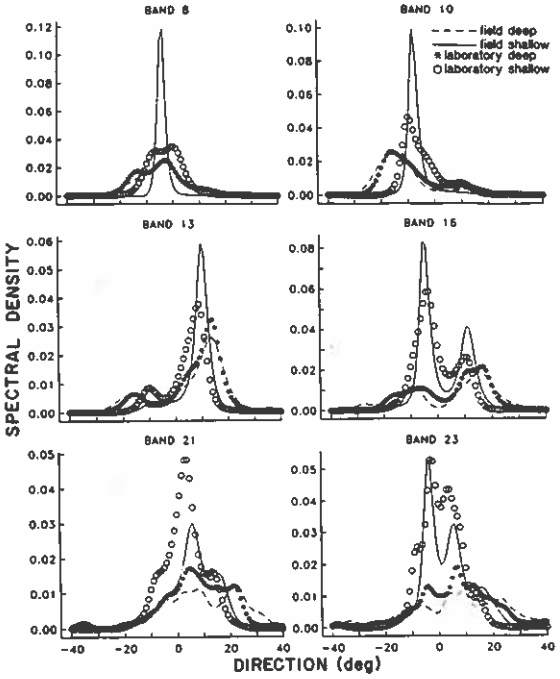


**FIG. 10. Directional Spectra for Selected Frequency Bands (Laboratory Deep $a/h$ = 0.055)**

water directional distributions are essentially identical. Similarly, the directional distributions for bands No. 10 (a low-power frequency band), 13 (a sea peak with a central direction from a different quadrant than that of the primary swell peak [band No. 8]), and 16 (the first harmonic of the primary swell peak) are accurately reproduced in the laboratory basin. Although deep-water power levels for the higher frequency bands in the laboratory are somewhat higher than the corresponding field values (Fig. 4), the directional distributions are qualitatively similar. For example, waves at band No. 21 have a broad directional distribution with most of the energy approaching the beach with angles between $-5°$ and 25° in both the field and laboratory.

The evolution of $E(f,\theta)$ observed in the field is discussed in detail in Freilich et al. (1990). As shown in Fig. 11 (same format as Fig. 9), the field and laboratory frequency-directional spectra are dominated by several peaks in shallow water. The three peaks centered at about $-4°$ correspond to the primary (band No. 8) and its first two harmonics (bands No. 16 and 23). For unknown reasons, the laboratory shallow directional spectrum for band No. 8 is not as narrow as that observed in the field. In both the field and the laboratory data, the harmonics are aligned with the direction of propagation of the primary (see Fig. 10 for details), consistent with nonlinear vector triad interactions (Freilich et al. 1990). The waves at harmonic frequencies with a direction ($-4°$) corresponding to that of the primary (band No. 8) are preferentially amplified during shoaling, while waves at the same

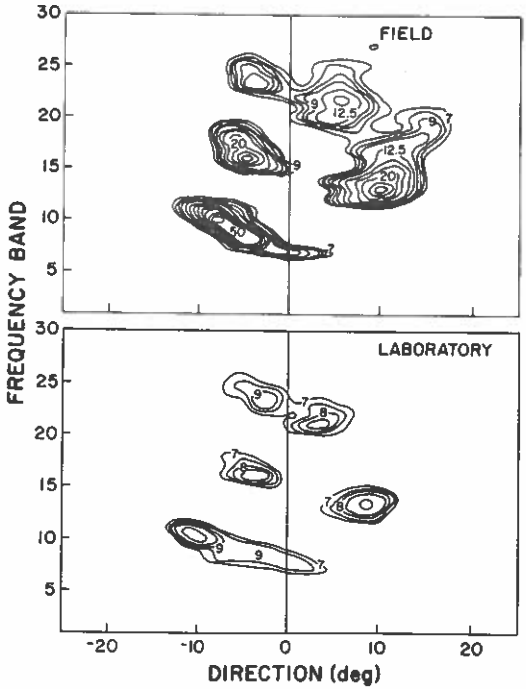


**FIG. 11. Measured Shallow-Water Frequency-Directional Spectra (Laboratory Deep $a/h$ = 0.055)**

harmonic frequencies, but other directions (e.g., the largest peak in band No. 16 deep-water directional spectrum is at about 11°) are much less influenced by nonlinearity. Similar preferential amplification of a $-4°$ peak occurs for the next higher harmonic (band No. 23).

The predominantly linear refraction of the low energy waves at bands No. 10 and 13 observed in the field is reproduced relatively well in the laboratory.

The shallow-water directional spectrum of band No. 21, the sum of the frequencies of bands No. 8 and 13, shows significant nonlinear effects in both the field (Freilich et al. 1990) and laboratory. In particular, waves with a direction of 6° are nonlinearly amplified during shoaling (Fig. 10), although the amplification is larger in the laboratory. These waves not only have the proper frequency for a triad interaction with waves at bands No. 8 and 13, but the wave number of the nonlinearly amplified waves ($\theta = 6°$) corresponds to the vector sum of the wave numbers of the directional peaks of bands No. 8 ($\theta = -4°$) and 13 ($\theta = 10°$). A two-dimensional model is required to study quantitatively differences between laboratory and field $E(f,\theta)$ at the shallow arrays. These differences may be associated with the different evolution distances and/or differences between the laboratory and field shallow-water array geometries. The result of the present qualitative comparisons is that all of the important features of the shoaled $E(f,\theta)$ in the field also occur in the laboratory for $a/h = 0.055$.

Frequency-directional spectra for other deep-water $a/h$ values in the lab-

oratory (not shown) are consistent with the expected nonlinear effects. For example, the smallest $a/h = 0.013$, which shows approximately linear amplification of the power spectrum [Fig. 6(*a*)], does not show enhanced energy at harmonics in directions colinear with the spectral peak. That is, in this case $E(f,\theta)$ evolves approximately linearly as well as $E(f)$ [Fig. 6(*a*)]. As $a/h$ is increased, the amount of colinear harmonic energy generally increases.

## Conclusions

A laboratory basin has been used to approximately reproduce field observations of a shoaling wave field that was broad banded in frequency and direction. The waves in the basin were generated in 34 cm depth by 60 paddles moved in a snake-like motion. A frequency-directional spectrum measured in 10-m water depth in the field was scaled and used as input to the wave generator. The resulting frequency-directional spectrum at the laboratory deep-water array (31 cm depth) was very close to the desired shape. The laboratory waves evolved similarly to those in the field, consistent with both rough scaling arguments and the predictions of a model based on the nonlinear Boussinesq equations. As predicted by the model, differences in the shoaled spectrum (with similar normalized incident wave heights) caused by different laboratory and field beach slopes could be reduced by altering the incident wave amplitude. With this compensation, the relative increase or decrease in spectral level at each frequency band observed during shoaling in the laboratory and field were nearly equal. Waves with frequencies corresponding to harmonics of the power spectral primary peak frequency received energy from the waves at the primary frequency. Higher-order statistics of the wave field, including bicoherence and water-surface elevation skewness and asymmetry, also evolved similarly in the field and the laboratory.

The directional spectra observed in 4 m depth in the field show significant nonlinear effects. In particular, harmonics of the power spectral primary peak frequency that are aligned with the direction of propagation of the primary are preferentially amplified, while waves at the same harmonic frequencies, but with nonaligned directions undergo evolution consistent with linear shoaling and refraction. This nonlinear evolution of harmonics is reproduced at the laboratory shallow array (12 cm depth). The nonlinear generation of nonharmonic waves satisfying vector triad resonance conditions (i.e., the generated wave had frequency and wave number equal to the sum of the frequencies and wave numbers of the interacting swell and sea) was also observed in both the laboratory and the field.

Although the beach slopes were different, and although there are many possible artifacts in the laboratory basin not found in the field (and vice versa), the shoaling process was remarkably similar.

## Acknowledgments

This research was funded by the physical oceanography program of the National Science Foundation. The field data collection was supported by the Office of Naval Research, Coastal Sciences. Numerical model calculations were conducted at the San Diego Supercomputer Center. Additional analysis was performed at the Jet Propulsion Laboratory, California Institute of Technology, under contract with NASA. The Office, Chief of Engineers, U.S. Army Corps of Engineers has authorized publication of this paper.

David Daily, Debbie Green, and Ken Hassenflug provided unequaled technical support during some very long days and nights at the directional basin.

## APPENDIX. REFERENCES

Abbott, M. B., Peterson, H. M., and Skovgaard, O. (1978). "On the numerical modelling of short waves in shallow water." *J. Hydr. Res.*, 16, 173–203.

Bailard, J. A., and Inman, D. L. (1981). "An energetics bedload model for a plane sloping beach: local transport." *J. Geophysical Res.*, 86, 2035–2043.

Bjiker, E. W., van Hijum, E., and Vallinga, P. (1976). "Sand transport by waves." *Proc. of the 15th Int. Conference on Coastal Engineering*, ASCE, 1149–1166.

Bowen, A. J. (1980). "Simple models of nearshore sedimentation; beach profiles and longshore bars." *The Coastline of Canada*, S. B. McCann, ed., Geological Survey of Canada.

Bowers, E. C. (1977). "Harbor resonance due to set-down beneath wave groups." *J. Fluid Mech.*, 79, 71–92.

Briggs, M. J., Borgman, L. E., and Outlaw, D. G. (1987). "Generation and analysis of directional spectral waves in a laboratory basin." *Paper OTC 5416*, Houston, Tex., 495–502.

Briggs, M. J., and Hampton, M. L. (1987). "Directional spectral wave generator basin response to monochromatic waves." *Technical Report CERC 87-6*, Coastal Engrg. Res. Ctr., USAE Waterways Experiment Station, Vicksburg, Miss., 1–90.

Elgar, S., and Guza, R. T. (1985*a*). "Shoaling gravity waves: A comparison between data, linear finite depth theory, and a nonlinear model." *J. Fluid Mech.*, 158, 47–70.

Elgar, S., and Guza, R. T. (1985*b*). "Observations of bispectra of shoaling surface gravity waves." *J. Fluid Mech.*, 161, 425–448.

Elgar, S., and Guza, R. T. (1986). "Nonlinear model predictions of bispectra of shoaling surface gravity waves." *J. Fluid Mech.*, 167, 1–18.

Elgar, S., Freilich, M. H., and Guza, R. T. (1990). "Model-data comparisons of moments of nonbreaking shoaling surface gravity waves." *J. Geophysical Res.*, 95, 16055–16063.

Freilich, M. H., and Guza, R. T. (1984). "Nonlinear effects on shoaling surface gravity waves." *Philos. Trans. R. Soc. London*, Royal Society of London, A311, 1–41.

Freilich, M. H., Guza, R. T., and Elgar, S. (1990). "Observations of nonlinear effects in directional spectra of shoaling surface gravity waves." *J. Geophys. Res.*, 95, 9645–9656.

Liu, P. L.-F., Yoon, S. B., and Kirby, J. T. (1985). "Nonlinear refraction-diffraction of waves in shallow water." *J. Fluid Mech.*, 153, 185–201.

Madsen, P., and Warren, I. (1984). "Performance of a numerical short-wave model." *Coastal Engineering*, 8, 73–93.

Mei, C. C., and Ünlüata, U. (1972). "Harmonic generation in shallow water waves." *Waves on beaches*. Edited by R. E. Meyer, Academic Press, New York, N.Y., 181–202.

Rygg, O. B. (1988). "Nonlinear refraction-diffraction of surface waves in intermediate and shallow water." *Coastal Engrg.*, 12, 191–211.

Stive, M. J. F. (1985). "A scale comparison of waves breaking on a beach." *Coastal Engrg.*, 9, 151–158.

Vincent, C. L., and Briggs, M. J. (1989). "Refraction-diffraction of irregular waves over a mound." *J. Waterway, Port, Coastal, and Ocean Engrg.*, ASCE, 115(2), 269–284.